



Intraformational unconformities as a record of late Miocene eustatic falls of sea level in the Pisco Formation (southern Peru)

Claudio Di Celma, Elisa Malinverno, Giulia Bosio, Karen Gariboldi, Alberto Collareta, Anna Gioncada, Walter Landini, Pietro Paolo Pierantoni & Giovanni Bianucci

To cite this article: Claudio Di Celma, Elisa Malinverno, Giulia Bosio, Karen Gariboldi, Alberto Collareta, Anna Gioncada, Walter Landini, Pietro Paolo Pierantoni & Giovanni Bianucci (2018) Intraformational unconformities as a record of late Miocene eustatic falls of sea level in the Pisco Formation (southern Peru), *Journal of Maps*, 14:2, 607-619, DOI: [10.1080/17445647.2018.1517701](https://doi.org/10.1080/17445647.2018.1517701)

To link to this article: <https://doi.org/10.1080/17445647.2018.1517701>



© 2018 The Author(s). Published by Informa UK Limited, trading as Taylor & Francis Group on behalf of Journal of Maps



[View supplementary material](#)



Published online: 07 Oct 2018.



[Submit your article to this journal](#)



Article views: 179











[View Crossmark data](#)



Citing articles: 2 [View citing articles](#)



Intraformational unconformities as a record of late Miocene eustatic falls of sea level in the Pisco Formation (southern Peru)

Claudio Di Celma ^a, Elisa Malinverno ^b, Giulia Bosio ^b, Karen Gariboldi ^c, Alberto Collareta ^{c,d}, Anna Gioncada ^c, Walter Landini ^c, Pietro Paolo Pierantoni ^a and Giovanni Bianucci ^c

^aScuola di Scienze e Tecnologie, Università di Camerino, Camerino, Italy; ^bDipartimento di Scienze dell'Ambiente e della Terra, Università di Milano-Bicocca, Milano, Italy; ^cDipartimento di Scienze della Terra, Università di Pisa, Pisa, Italy; ^dDottorato Regionale in Scienze della Terra Pegaso, Pisa, Italy

ABSTRACT

Field mapping and sedimentological study of outcrop sections exposed along the Ica River valley permitted the establishment of a regional allostratigraphic framework for the upper Miocene portion of the Pisco Formation. The stratigraphy of the studied interval is illustrated using a new 1:20,000-scale geological map which reveals that this formation is a cyclical sedimentary succession composed of three fining-upward allomembers. The bounding surfaces defining each allomember are transgressively modified subaerial unconformities. They converge and merge landward into a single composite surface representing the time-transgressive lower boundary of the Pisco Formation. Accordingly, the extent of the stratigraphic gap associated with the basal unconformity varies significantly throughout the basin and increases toward the basin margins. The timing of allomember-bounding surfaces coincides with that of major oxygen-isotope maxima in the deep-sea oxygen isotopic record and matches the ages of eustatic sequence boundaries identified elsewhere, indicating glacio-eustatic falls due to the growth of Antarctica ice sheets as a viable mechanism for their development.

ARTICLE HISTORY

Received 26 December 2017
Revised 11 July 2018
Accepted 27 August 2018

KEYWORDS

Pisco Formation; late Miocene; allostratigraphy; glacio-eustasy

1. Introduction

The upper Miocene to Pliocene Pisco Formation of southern Peru is famous for its fossiliferous sites and the very large number of high-quality fossil marine vertebrates it contains (e.g. Bianucci, Di Celma, Urbina, & Lambert, 2016; Collareta et al., 2015; Collareta et al., 2017; Esperante, Brand, Chadwick, & Poma, 2015; Gioncada et al., 2016; Lambert et al., 2010, 2015; Lambert, Bianucci, Urbina, & Geisler, 2017; Landini, Altamirano-Sierra, et al., 2017; Landini, Collareta, et al., 2017; Marx, Collareta, et al., 2017; Marx, Lambert, & de Muizon, 2017). Despite numerous significant paleontological discoveries and the studies dedicated to the favourable diagenetic conditions leading to the exceptional preservation of bones (Brand, Esperante, Chadwick, Porras, & Alomía, 2004; Esperante, Brand, Nick, Poma, & Urbina, 2008; Gariboldi et al., 2015; Gioncada, Gariboldi, et al., 2018; Gioncada, Petrini, et al., 2018), so far this sedimentary succession has been the subject of few modern sedimentological or stratigraphic studies (Brand, Urbina, Chadwick, DeVries, & Esperante, 2011), which means that the relative positions of its vertebrate fossil localities remains tentative and, at least in part, still unknown.

In the last few years, the stratigraphic architecture of the Pisco Formation has been documented in local

studies (Di Celma et al., 2017; Di Celma, Malinverno, Cantalamessa, et al., 2016; Di Celma, Malinverno, Gariboldi, et al., 2016) and constrained with biostratigraphic and geochronologic studies (Bosio et al., in press; Gariboldi, 2016; Gariboldi et al., 2017). This paper forms part of this ongoing attempt to create a refined chronostratigraphic model for the vertebrate fossil localities of the Pisco Formation (Bianucci, Di Celma, Collareta, et al., 2016; Bianucci, Di Celma, Landini, et al., 2016) and illustrates a high-resolution outcrop-based allostratigraphic framework for upper Miocene sediments of the Pisco Formation exposed along the western bank of the Ica River. Such a detailed stratigraphic analysis provides both the physical and temporal framework within which a number of broader issues concerning patterns of marine vertebrate evolution, speciation, and extinction events can be addressed.

Within strata of the Pisco Formation, some of the most important shifts in composition and diversity of the marine vertebrate community occur across a series of basin-wide intraformational unconformities (Di Celma et al., 2017). At present, the causes that drove these turnover events are uncertain and a causal link between them and the development of the

unconformities has yet to be established. Here we investigate the nature of the unconformities and explore a possible relationship between them and eustatic sea-level oscillations related to global cooling. During the middle Miocene, indeed, Earth's climate transitioned from a prolonged phase of global warmth (the middle Miocene Climatic Optimum) into a Middle to late Miocene stepwise climate cooling phase (the middle Miocene Climate Transition) (Flower & Kennett, 1994; Holbourn, Kuhnt, Clemens, Prell, & Andersen, 2013). This prominent cooling phase represents one of the major steps in Cenozoic climatic evolution (e.g. Zachos, Shackleton, Revenaugh, Pälike, & Flower, 2001) and was punctuated by several short-lived episodes of glaciations, the Mi-Events of Miller, Wright, and Fairbanks (1991), and concomitant eustatic lowerings reflecting increased continental ice volume on Antarctica.

The objectives of the present contribution are: (i) to identify Miocene unconformities in the Pisco Formation; (ii) to trace them, and the sedimentary packages in between, over the entire studied area; and (iii) to assess the nature of the basin-wide discontinuities that have been used to outline the Pisco allomembers by comparing their ages with the timing of eustatic sea-level lowstands inferred from Middle and late Miocene oxygen isotope records.

2. Geological and stratigraphic setting

The Peruvian margin is generally recognised as a long-lived convergent margin, with the oceanic Farallon/Nazca Plate subducting below the western margin of South America at least since the beginning of the Jurassic (Coira, Davidson, Mpodozis, & Ramos, 1982). The subduction of normal oceanic lithosphere and collision of the aseismic Nazca Ridge beneath this part of the forearc zone have been associated with a wide range of effects on the leading edge of the overriding South America continent, including long-term subsidence driven by basal tectonic erosion, rapid crustal uplift and exhumation, and the development of a composite transform-convergent margin dominated by extensional and strike-slip tectonic activity (Bishop et al., 2017; Clift, Pecher, Kukowski, & Hampel, 2003; Dunbar, Marty, & Baker, 1990; Hampel, Kukowski, Bialas, Huebscher, & Heinbockel, 2004; Hsu, 1992; Kulm, Resig, Thornburg, & Schrader, 1982; León, Aleman, Torres, Rosell, & De La Cruz, 2008; Macharé & Ortlieb, 1992). According to Thornburg and Kulm (1981), two trench-parallel structural highs were formed on the continental shelf and upper slope of the Peruvian margin during late Cretaceous-early Paleogene time, namely the Outer Shelf High and the Upper Slope Ridge. These two structural highs subdivided the Peruvian offshore into a chain of fault-bounded

sedimentary basins, which formed in response to prolonged extension and subsidence since the middle-late Eocene (Viveen & Schlunegger, 2018) and may be separated into an inner set of shelf basins and a seaward set of slope basins (Figure 1). In southern Peru, the onshore (East) Pisco Basin is separated from the adjacent West Pisco Basin, which is situated on the slope, by the Outer Shelf High.

The Pisco Basin contains a sequence of Eocene to Pliocene sedimentary strata, nonconformably overlying Precambrian to lower Cretaceous basement rocks (Kulm et al., 1982; León et al., 2008; Mukasa & Henry, 1990; Thornburg & Kulm, 1981). From its base upward, the sedimentary fill consists of the Paracas Formation, the Otuma Formation, the Chilcatay Formation, and the Pisco Formation (DeVries, 1998; DeVries & Jud, 2018; DeVries, Urbina, & Jud, 2017; Dunbar et al., 1990). These formations are bounded by regionally bevelling, conglomerate-mantled unconformities that are locally accompanied by angular discordances and, therefore, they would be better defined as alloformations (NACSN, 2005).

The basin fill is variously folded and faulted and deformation is generally less intense as one moves upward through the sedimentary succession. In the Pisco Formation faults display dip angles mostly comprised between 75° and 85°. Kinematic indicators suggest that all of the faults are either pure normal faults or have a minor strike-slip component (Rustichelli, Di Celma, Tondi, & Bianucci, 2016). These faults display two main ranges of orientation, with the large majority of them having a NW–SE orientation and the remainder generally striking NE. Along these faults the displacement is generally minimal (metres to tens of metres) and also varies along strike, occasionally tipping out into a fracture with no displacement. Most of the fault zones are marked by an abundance of gypsum filled veins (Rustichelli, Di Celma, Tondi, Baud, & Vinciguerra, 2016).

3. Methods

The stratigraphic architecture of the study interval is illustrated using a new geological map (Main Map), which encompasses an area of about 200 km², and two northwest-southeast and south-north trending geological cross-sections. Field mapping has been carried out at 1:10,000 scale, however the final map has been compiled at 1:20,000 scale. The allostratigraphic approach employed for the purpose of the present study is based on recommendations of the North American Commission on Stratigraphic Nomenclature (NACSN, 2005). However, the allomembers defined herein are considered to be informal stratigraphic units, designated by letters and numbers rather than formally defined names. By emphasizing the importance of chronostratigraphically significant

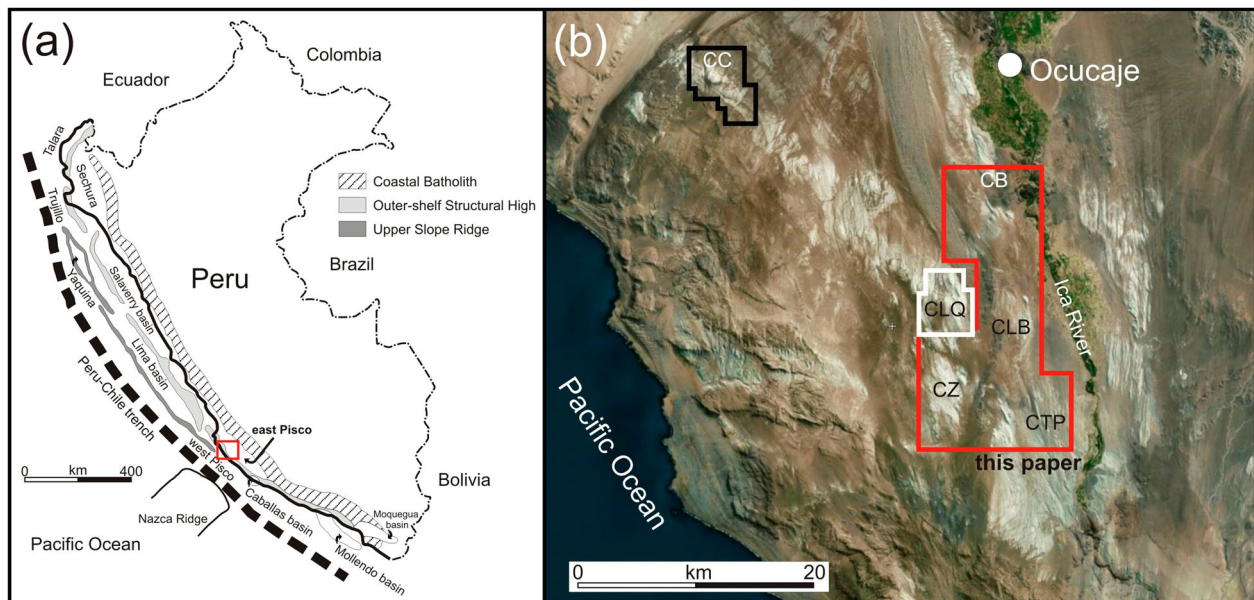


Figure 1. Location maps of the present study. (a) Regional geographic context; (b) annotated air photo image (red box in (a) showing locations of the study area (red frame) and location of the four stratigraphic sections measured at Cerro las Tres Piramides (CTP), Cadenas de los Zanjones (CZ), Cerro la Bruja (CLB), and Cerro Blanco (CB). The areas in the black frame (Cerro Colorado, CC) and in the white frame (Cerro los Quesos, CLQ) have been mapped by Di Celma, Malinverno, Gariboldi, et al. (2016) and Di Celma, Malinverno, Cantalamessa, et al. (2016), respectively.

discontinuities, the allostratigraphic approach has facilitated correlation of discontinuity-bounded stratal units and permitted an appreciation of the genetic relationships between coeval depositional settings. The bounding discontinuities that have been used to define the Pisco allomembers are represented by composite subaerial unconformity/marine-generated transgressive surfaces that, in general, are characterised by an abrupt transition from finer-grained offshore diatomites to coarser-grained shoreface sandstones. Age control for Pisco strata and bounding unconformities relies on the integration of recently published biostratigraphic data and $^{40}\text{Ar}/^{39}\text{Ar}$ age estimates (Gariboldi et al., 2017).

The allostratigraphic scheme presented in this paper builds upon the original allostratigraphy established by Di Celma, Malinverno, Cantalamessa, et al. (2016) and Di Celma, Malinverno, Gariboldi, et al. (2016) for the Pisco Formation at Cerro Colorado and Cerro Los Quesos. In order to identify the depositional settings, to define stratigraphic surfaces, and to delineate genetic units, four detailed sedimentary sections (totalling some 710 m of measured stratigraphy) were logged at the decimetre scale through the exposed succession. For every single bed, lithology, colour, composition, texture, sedimentary structures, amount and type of bioturbation, palaeocurrent directions, and macrofossil content have been described. These four sections were successfully correlated by walking out a series of distinctive physical stratigraphic markers and bounding erosion surfaces in the field, by visually tracing them along outcrop photopanels, and by using high-resolution Google Earth imagery.

4. Description of map units

The study area is located along the eastern, internal margin of the basin, where the infilling sedimentary succession becomes stratigraphically incomplete and only the Miocene Chilcatay and Pisco formations occur at the surface, resting directly on the eroded surface of the pre-Cenozoic basement. The Eocene-Oligocene strata of the Otuma Formation are widely exposed outside of the southern and south-southeastern boundaries of the map area, but their extension in the subsurface of the mapped area is virtually unknown and remains tentative. As a consequence, the description provided below will focus only on the exposed stratigraphic units.

4.1. Basement

All the pre-Cenozoic units are grouped together under this title. Within the study area, the basement rocks consist of a complex assemblage of lower Palaeozoic gabbroic to granitoid rocks forming the San Nicolás batholiths (Mukasa & Henry, 1990), intruding a Precambrian metamorphic complex known as the Arequipa massif and covered by Jurassic volcano-sedimentary rocks of the Guaneros Formation. The Guaneros Formation consists of volcanoclastic rocks with andesitic to rhyolitic composition deriving from a Jurassic calcalkaline volcanic arc, interbedded with calcareous sediments (León et al., 2008). In the study area, exposures of the basement rocks are limited and only occur between Cerro la Bruja and Cerro Blanco.

4.2. Chilcatay Formation

Sediments of the Chilcatay Formation rest either with angular unconformity on the Otuma Formation or directly on the undulatory surface of the basement rocks. Over much of the study area, Chilcatay strata dip gently to the northeast and are subdivided by an intraformational unconformity into two distinctive sediment wedges (Figure 2; Di Celma et al., 2018). The lower unit displays a stratigraphic thickness in excess of 65 m and comprises a package of massive or weakly bedded, heavily bioturbated, sandy siltstones with disperse comminuted skeletal debris. These sandy siltstones underlie and landward interfinger (from southwest to northeast) with a package of seaward-dipping, 20 m-thick clinofomed grainstones. The clinostratified beds display decimetric thickness and, generally, their dip directions indicate a distinct mode southwestward. Reworked barnacle plates, pectinids and oysters account for a large portion of the highly degraded skeletal fraction, emphasising the non-tropical character of these mixed siliciclastic-carbonate rocks (compositional mixing *sensu* Chiarella, Longhitano, & Tropeano, 2017) and suggesting their development within a shallow-marine carbonate factory. Similar heterozoan carbonate wedges with seaward dipping, steep clinofoms have been documented by Pomar and Tropeano (2001) and Massari and D'Alessandro (2012). These authors interpreted the clinofoms as the product of offshore-directed storm waves and currents that shed off the skeletal materials from a shoreface carbonate factory and accumulated them along a steep clinofomed ramp, within an offshore-transition setting. In this scenario, the underlying and laterally adjacent sub-horizontal sandy siltstones are interpreted to reflect deposition of the suspended load within a proximal offshore setting.

The clinostratified body of mixed siliciclastic-carbonate rocks is unconformably overlain by a fining-upward sedimentary succession that is about 10 m thick at Cerro las Tres Piramides and about 25 m thick at Cerro Yesera de Amara. This sedimentary unit comprises a 3.5 m-thick package of massive, medium-grained sandstones overlain by a package of massive siltstones that represent shoreface and outer shelf depositional settings, respectively. A volcanic ash layer sampled in the upper portion of massive siltstones, just 1 m below the erosional contact with the overlying Pisco Formation, provided an $^{40}\text{Ar}/^{39}\text{Ar}$ age of 18.02 ± 0.07 Ma, whereas biostratigraphic data from the same stratigraphic interval seem to indicate a slightly younger age (Di Celma et al., 2018).

4.3. Pisco Formation

The Pisco Formation is a regionally extensive stratal unit recording the final widespread marine incursion

into the Pisco Basin. Within the study area, its strata form a northeastward dipping monocline and consists mainly of marine diatomites with subordinate siltstones and sandstones. The base of the Pisco Formation has a composite nature and includes at least three regionally mappable unconformities (Figure 3a), termed PE0.0 through PE0.2 in ascending order, which converge and merge landward (i.e. to the northeast) to form a single diachronous surface (PE0). The stratal configuration below and above this composite surface varies with position within the basin and is most commonly that of an angular unconformity where it overlies older sediments of the Chilcatay Formation, or it is a nonconformity where it rests directly on crystalline basement rocks (i.e. along the basin margins). A high-resolution allostratigraphic approach, based on mapping of three basin-wide unconformities, revealed that the investigated interval is composed of three allomembers (named alphanumerically P0, P1, P2 from older to younger). The three allomembers are thought to be equivalent to depositional sequences separated by transgressively-modified subaerial unconformities, associated with shifts in base level (Di Celma et al., 2017).

Internally, each allomember preserves a record of water-depth change during deposition and displays an overall fining-upward trend of facies associations marking a gradual vertical shift from shoreface to offshore deposits. None of the allomember-bounding discontinuities shows evidence of subaerial exposure, although each marks an abrupt shallowing and seaward shift in facies. These surfaces are penetrated by a *Thalassinoides*-dominated *Glossifungites* ichnofacies (Figure 3b), indicating the erosional exposure of sedimentary firmgrounds that were subsequently colonised by burrowing animals (e.g. MacEachern, Raychaudhuri, & Pemberton, 1992). Directly overlying the *Glossifungites*-demarcated surfaces is a relatively thin (up to 0.4 m thick), coarse-grained layer including a variable mixture of pebble-size phosphatic nodules, well-rounded pebble- to boulder-size basement clasts, cobble-size clasts of dolomite-cemented mudstone showing bivalve borings, internal moulds of gastropods and articulated bivalves, shark teeth, and polished bone fragments (Figure 3a and b). This coarse-grained layer is regarded as a condensed transgressive lag produced in the shoreface by low net sedimentation rates during shoreline retreat (e.g. Boessenecker, Perry, Schmitt, & Farke, 2014; Di Celma, Ragaini, Cantalamessa, & Curzio, 2002; Föllmi, 2016; Grimm, 2000). A sand-prone facies association is invariably found immediately above the aforementioned transgressive lag. It comprises yellow-weathering, intensely bioturbated, fine- to very fine-grained sandstones containing elongated, U-shaped, sand-filled gutter casts (Figure 3c). These structures characterise sedimentation during storms and are of

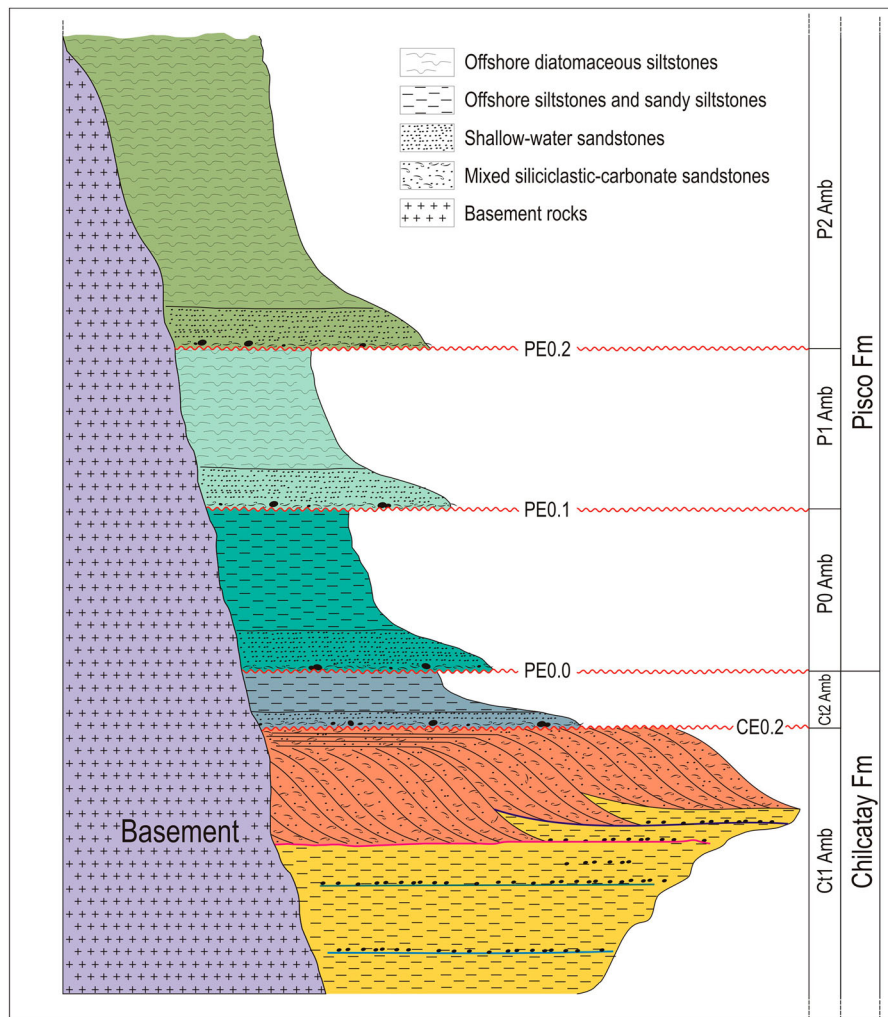


Figure 2. Schematic stratigraphic section of Pisco Formation and adjacent rocks. For simplicity, erosion surfaces have been designated 'E' with a preceding letter indicating the relevant formation (C = Chilcatay, P = Pisco) and numbers designating successively higher stratigraphic surfaces. Accordingly, PE0.0, PE0.1, PE0.2 indicate successively younger erosion surfaces in the Pisco Formation. These three unconformities converge and merge landward into a single surface (informally referred to as PE0) representing the composite lower boundary of the Pisco Formation. The resulting allomembers (Amb) have been named for their lower bounding surface. Thus, the P0 allomember refers to strata lying between the PE0.0 unconformity and the next higher unconformity (PE0.1). The vertical scale is only indicative of thickness of sediment packages between unconformity surfaces.

particular sedimentological significance for the interpretation of nearshore depositional environments (i.e. Chiocci & Clifton, 1991; Leckie & Walker, 1982; Myrow, 1992). The basal sandstones grade up into finely laminated gray-white diatomaceous mudstones recording deposition by suspension settling of diatom frustules in a low-energy offshore setting (Figure 3d). Subordinate lithologies include volcanic ash layers, more resistant dolomite-cemented mudstones, fine- to medium-grained sandstones, and phosphatic nodule beds forming laterally continuous ledges in steep slopes. Traced northeastward to outcrops between Cerro la Bruja and Cerro Blanco, the diatomaceous mudstones gradually give way to laterally adjacent storm-influenced shoreface sandstones, displaying swaley cross-stratification, large-scale unidirectional cross-bedding, and small-scale, gravel-filled gutter casts oriented perpendicular to the palaeoshoreline (Figure 3e–g).

4.3.1. P0 allomember

The P0 allomember is bounded at the base by PE0.0 and at the top by PE0.1 (Figure 4a and b). This stratal unit is confined to the southern part of the study area, where it attains its greatest thickness (about 40 m) at Cerro las Tres Piramides. Based on physical stratigraphic relationships, it pinches out toward the north and the west accompanied by the merging of the PE0.0 and PE0.1 bounding surfaces.

At present, due to the lack of direct biostratigraphic and radiometric data, the age of P0 is constrained by the $^{40}\text{Ar}/^{39}\text{Ar}$ radiometric ages for volcanic ash beds in the youngest sediments of the underlying Chilcatay Formation at Cerro Yesera de Amara (18.02 ± 0.07 Ma, Di Celma et al., 2018) and for the onset of deposition of the overlying P1 allomember strata at Cerro Colorado (9.10 ± 0.04 Ma, Gariboldi et al., 2017) and at Cerros Cadenas de los Zanjones (9.00 ± 0.02 Ma, Di Celma et al., 2017).



Figure 3. (a) Detail of the unconformity between the P0 and P1 allomembers at Cerro las Tres Piramides (black dotted line). This surface places coarse-grained sediments composed of tightly packed phosphate pebbles, basement clasts, shark teeth, and polished bones surrounded by a sandy matrix (above) in direct and erosive contact with diatomite mudstones (below); (b) below the surface, frequent *Thalassinoides* burrows are filled with small phosphate nodules; (c) close up of sand-filled gutter casts in the nearshore facies at the base of the P2 allomember. They occur parallel to each other as discrete scours that are usually less than 1.50 m in width and 0.5 m deep. In cross section, these erosional structures display a gently (concave up) curved base and outlines that flare upward. Internally, they are filled with slightly sagging sandy laminae that either drape the margins concordantly or pinch out discordantly against them (Cadenas de los Zanjones); (d) finely laminated diatomites (P2, Cerro Hueco la Zorra); (e) close up view of multiple gravel-filled gutter casts at the base of a gravel bed in nearshore facies. Typically, these linear features are 0.20–0.25 m wide and 0.15 m deep and laterally connected. Lateral spacing is regular, at distances of about 0.3 m. Their cross-sectional shape is generally symmetrical and some have walls with stepped outlines. Gutters show a strongly preferred NE orientation, nearly perpendicular to the inferred shoreline trend. Gutters show a strongly preferred NE orientation, nearly perpendicular to the inferred shoreline trend. The infill consists of pebble-size phosphatic nodules set in a well-sorted, medium- to coarse-grained sand (base of P2, Cerro Blanco); (f) swaley cross-stratification in fine-grained sandstone produced by storm-induced oscillatory and combined flows (base of P2, Cerro Blanco); (g) oblique view of trough cross-stratification produced in medium- to coarse-grained bioclastic sandstones by migration of lunate bedforms (base of P1, Cerro la Bruja).

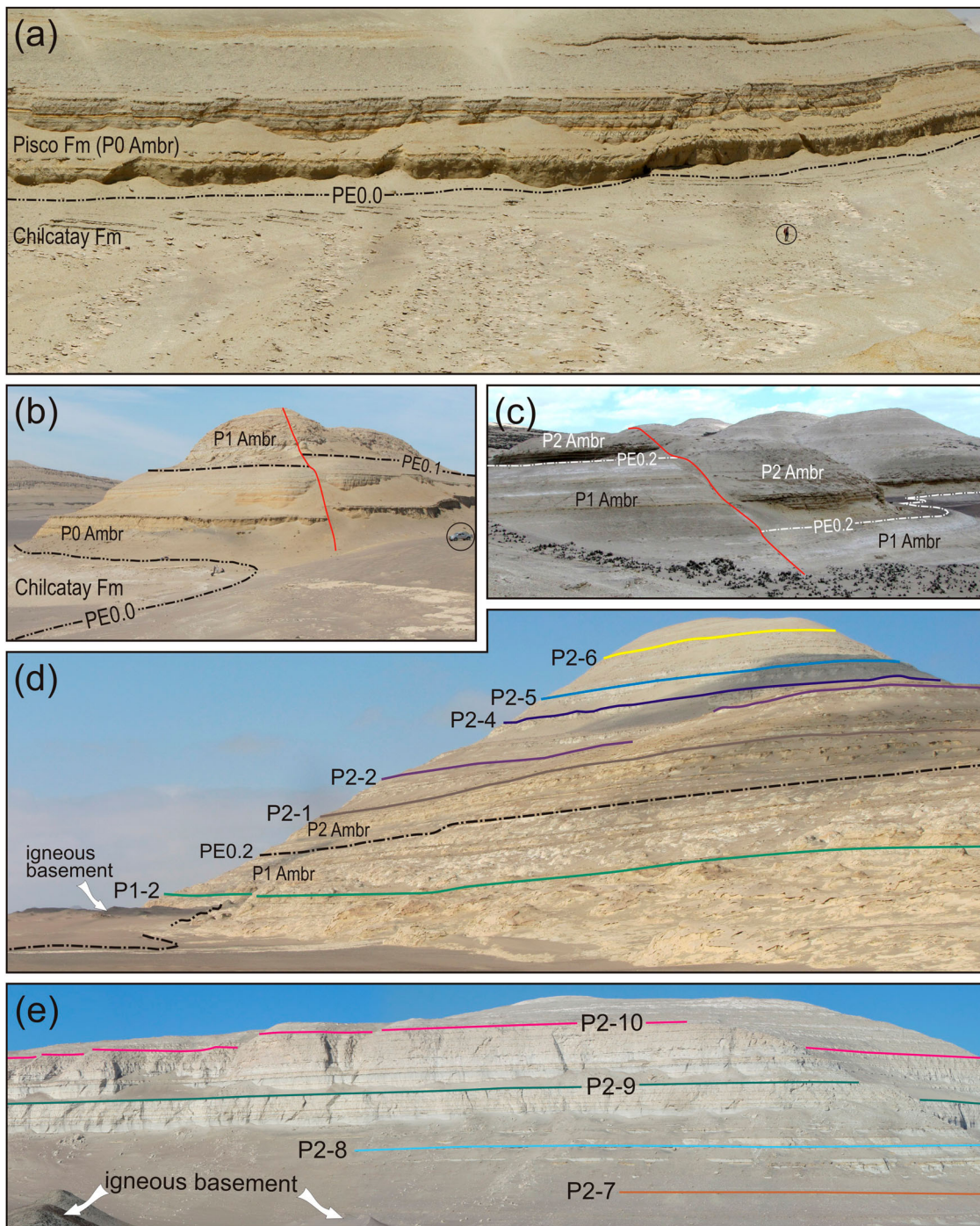


Figure 4. Annotated panoramic photographs of Pisco outcrops showing: (a) eastward view of the upper part of the Chilcatay Formation overlain along an unconformably contact by the marine deposits of the P0 allomember at Cerro los Tinajones (circled geologist for scale); (b) the vertically staked marine deposits of P0 and P1 at Cerro Submarino (circled car for scale); (c) outcrop view of sediments in the vicinity of the unconformity surface between allomembers P1 and P2 (PE0.2) at Cadenas de los Zanjonés; (d) crystalline basement nonconformably overlain by P1 strata and ledge-forming marker beds within P1 and P2 (Cerro la Bruja); (e) crystalline basement nonconformably overlain by P2 strata and ledge-forming marker beds serving as formidable correlation tools over wide areas within P2 (Cerro Hueco la Zorra).

4.3.2. P1 allomember

The P1 allomember is bounded at the base by PE0.1 and at the top by PE0.2 (Figure 4b–d). The geological mapping suggests that this unit onlaps onto the underlying P0 strata and basement rocks and progressively oversteps them from southwest to northeast. The P1 allomember is exposed throughout the entire study area and is about 100 m thick at Cerros Cadenas de los

Zanjonés, where a continuous stratigraphic section can be measured. To help stratigraphically subdividing this unit, two marker beds, namely P1-1 and P1-2, have been correlated across part of the study area (Figure 4d).

4.3.3. P2 allomember

This allomember, which is more than 210 m thick at Cerro la Bruja, has 10 ledge-forming marker beds

(designated P2-1 through P2-10 in ascending order, Figure 4d and e) being traceable across most of the central and northern portions of the study area and, at least in part, westward into the sedimentary succession exposed at Cerro los Quesos (Di Celma et al., 2017). Careful mapping of these marker beds between Cerro la Bruja and Cerro Blanco shows that the shallow-water strata of the P2 sequence extend beyond the northern limit of the present study area and onlap an unconformity surface cut across the P1 sequence, which they overstep north of Cerro el Brujito to onlap onto basement crystalline rocks. Lateral tracing of the same marker beds in the southern portion of the study area, between Cerros Cadenas de los Zan-jones and Cerro la Mama y la Hija, is hampered by the distance of these localities and the presence of extensive sediment cover.

5. Discussion

5.1. Origin and timing of erosional unconformities and correlation to global events

Diatom biostratigraphy combined with available $^{40}\text{Ar}/^{39}\text{Ar}$ radiometric ages indicate that strata of the P1 allomember in the study area were deposited between about 9.5 and 8.9 Ma, whereas those of the P2 allomember are younger than 8.5 Ma (Gariboldi et al., 2017). A comparison between the estimated ages of allomember-bounding unconformities in the Pisco Formation and a glacio-eustatic proxy afforded by deep-sea oxygen isotopic records indicates that, within the resolution of our age model, PE0.2 approximates the drop in sea level recognised as the Mi7 event of Miller et al. (1991), an isotopic maximum dated at 8.7 Ma by Miller et al. (1998) and Westerhold, Bickert, and Röhl (2005). The PE0.1 unconformity correlates reasonably well with the Mi6 oxygen isotope maximum dated at 10.3 Ma by Miller et al. (1998) and astronomically dated at 10.4 Ma by Turco, Hilgen, Lourens, Shackleton, and Zachariasse (2001) and Westerhold et al. (2005). Assuming that this correlation between the studied PE0.1 and PE0.2 unconformities and the eustatic curve derived from deep-sea oxygen isotope records is correct and, therefore, that these breaks in deposition have an eustatic (global) rather than tectonic (local) origin, we speculate that the PE0.0 unconformity reflects the Mi5 event, an isotopic maximum dated at 11.7 Ma by Miller et al. (1998) and astronomically at 11.4 and 11.7 Ma by Turco et al. (2001) and Westerhold et al. (2005), respectively (Figure 5). In this frame, intermittent periods of subaerial exposure during deposition of the Pisco Formation were likely produced by recurring third-order (0.5–3 m.y.) eustatic oscillations with the rate of eustatic fall exceeding that of long-term tectonic subsidence. As a main result, the several hundred metres thick sediments of the Pisco

Formation reflect accommodation space produced by a combination of moderate subsidence rates and eustatic sea-level fluctuations.

An additional support to the eustatic origin for these allomember-bounding surfaces would be the similar timing of the unconformities in different ocean basins. Comparison of ages of depositional breaks in the Pisco Formation with ages of seismic sequence boundaries identified and dated in the Bahamas (Eberli, Anselmetti, Kroon, Sato, & Wright, 2002; ODP Leg 166) indicates that the timing of the PE0.1 and PE0.2 unconformities is remarkably similar with the timing of eustatic sequence boundaries lettered H (9.4 Ma) and G (8.7 Ma) along the Bahamas Transect, respectively.

Considering the above assumption and available chronological constraints, the time represented by the erosional unconformity interposed between the youngest sediments of the Chilcatay Formation (18.02 ± 0.07 Ma) and the oldest sediments of the Pisco Formation (11.7 Ma) is about 6.3 m.y. This long hiatus in the stratigraphic record indicates a prolonged phase of subaerial exposure and erosion of this marginal basin and possibly reflects a widespread pulse of uplift and compression related to the Quechua 1 tectonic event (Viveen & Schlunegger, 2018) exacerbating the effects of the long-term global lowering of sea level recorded during the the middle Miocene Climate Transition. The most recent estimates for the amplitude of the eustatic changes during this period indicate that the sea-level fell about 53–69 m between 16.5 and 13.9 Ma (John et al., 2011) and 50 ± 5 m between 13.6 and 11.4 Ma (John, Karner, & Mutti, 2004). As such, the Pisco Formation records a subsequent, widespread marine transgression and re-flooding of the forearc basin.

5.2. Allomember stacking pattern

The evidence of an eustatic origin for the allomember-bounding unconformities in the Pisco Formation does, obviously, not imply that the regional tectonic activity did not affect the overall stratigraphic architecture of this unit. Within the study area, the PE0.1 and PE0.2 surfaces onlap onto the older PE0.0 surface in a broadly northeasterly direction, merging into a composite PE0 unconformity. Accordingly, the intervening P0, P1, and P2 allomembers taper progressively to the northeast and overstep each other to lap out against the pre-Cenozoic crystalline basement, forming a set of retrogradationally stacked stratal wedges. This architectural pattern, suggesting a steady increase in the accommodation space, is indicative of deposition during a long-term period of relative sea-level rise punctuated by repeated sea-level falls and is interpreted as the product of third-order eustatic sea-level changes superimposed on prolonged extension and relatively uniform subsidence (Viveen & Schlunegger, 2018).

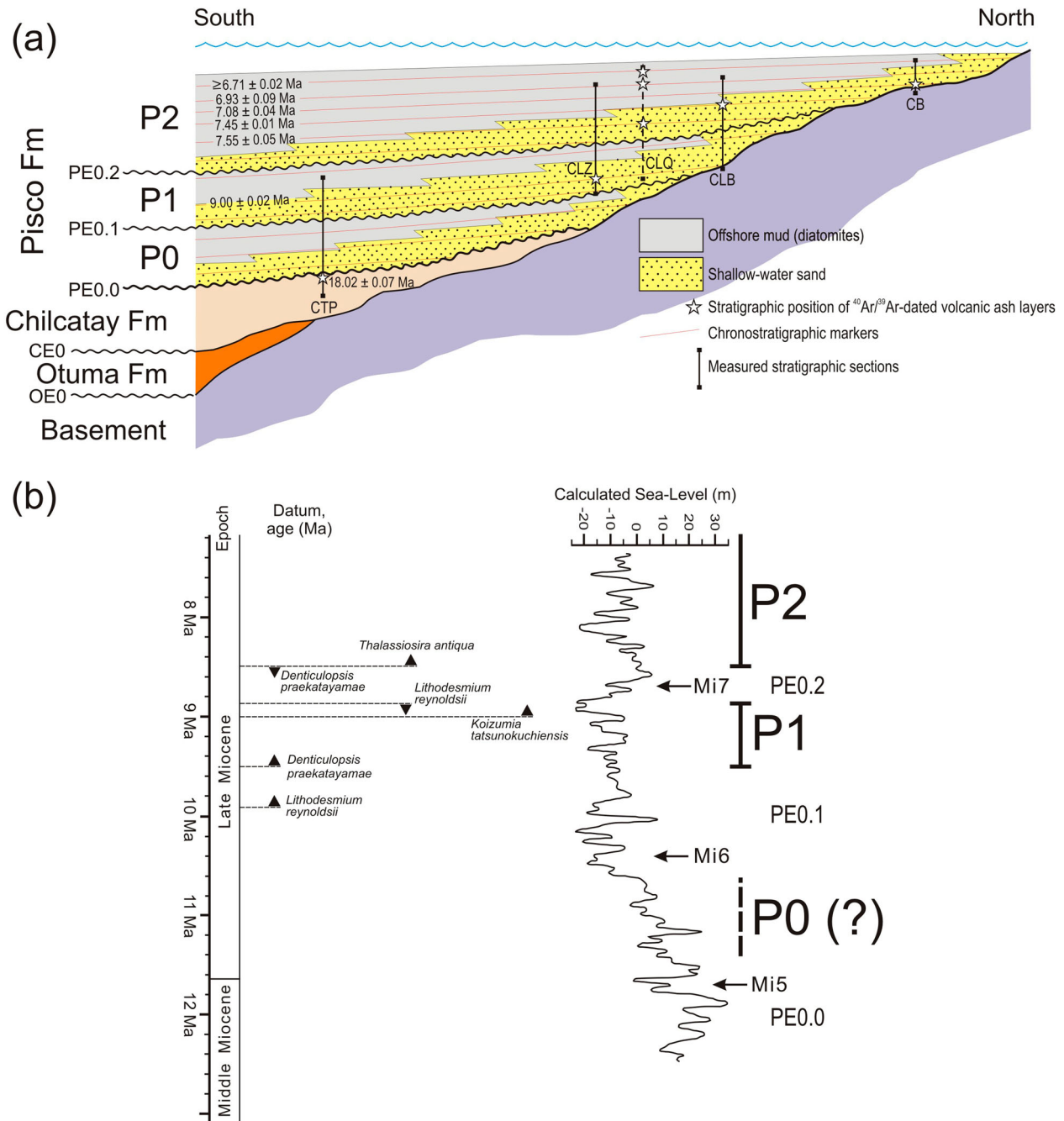


Figure 5. (a) Schematic, dip-oriented stratigraphic diagram for the Pisco Formation (not in scale) showing the position of the stratigraphic sections on which the diagram is based (vertical black lines). Geochronologic data from these sections were supplemented by additional $^{40}\text{Ar}/^{39}\text{Ar}$ radiometric ages from Cerro los Quesos (CLQ, vertical dashed line). The Pisco Formation exhibits pronounced thinning to the northeast with component allomembers onlapping onto the basal composite surface PE0 and arranged in a retro-gradational pattern, progressively offset to the northeast. The marine erosion surfaces that bound Pisco sequences, namely PE0.0, PE0.1, and PE0.2, were formed as a result of wave erosion in a transgressing shoreline following sea-level lowstands and, therefore, will be close to planar and inclined slightly seaward. Red lines indicate chronostratigraphic markers; (b) correlation of Pisco allomembers with late Miocene sea-level fluctuations by using integrated biostratigraphic and geochronologic data from Gariboldi et al. (2017). Diatom biostratigraphy revised following most recent publications on Equatorial Pacific diatom biostratigraphy (mostly Barron, 2003). Calculated sea-level curve from Westerhold et al. (2005).

6. Conclusions

A systematic analysis of the sedimentological and stratigraphic features of the outcrop belt exposed along the western bank of the Ica River valley permitted the establishment of a regional allostratigraphic framework for the upper Miocene portion of the Pisco Formation. Coplanar subaerial unconformity/marine-generated

transgressive surfaces, designated PE0.0, PE0.1 and PE0.2, can be traced throughout the entire study area and provide a basis for defining the presence of three informal allomembers, designated P0 through P2, in the order of a few tens to hundreds of metres thick. These allomembers display repetitive vertical facies successions representing a spectrum of storm-

influenced shoreface to offshore environments laid down during the relative rise of sea-level cycles.

In the study area, the Pisco Formation forms a northeastward-thinning wedge and its composite lower boundary steps up-section from the base of the P0 allomember in the southwest, through that of the overlying P1, to coincide with the base of P2 to the northeast (paleolandward). Accordingly, the extent of the stratigraphic gap associated with the basal unconformity varies significantly throughout the basin and increases toward the basin margins.

At this stage, the underlying control on these fluctuations of sea level is in part speculative. However, combined biostratigraphic and geochronologic age constraints indicate that at least two bounding unconformities developed near discrete glacial intervals inferred from deep-sea oxygen isotope records, suggesting a causal link between the observed depositional cyclicity and third-order late Miocene changes in global sea level caused by the waxing and waning of the Antarctic ice sheet. On the basis of available age control, unconformities PE0.1 and PE0.2 appear to correlate with isotopic maxima observed at about 10.4 and 8.7 Ma, respectively. We speculate that the PE0.0 unconformity at the base of the P0 allomember might correlate with the isotopic maxima observed at 11.7 Ma.

As a consequence of third-order glacio-eustatic fluctuations in sea-level acting in concert with relatively uniform subsidence rates, the study area was alternatively exposed and submerged, leading to development of bounding subaerial unconformities during glacial lowerings of sea level and deposition of allomembers during interglacial sea-level rises. Over the long-term, this combination of eustatic fluctuations and basin subsidence resulted into a punctuated relative sea-level rise, with P0, P1 and P2 allomembers stacked in a retrogradational, overlapping configuration onto the underlying Chilcatay Formation and the pre-Cenozoic basement.

Software

The geological map and associated geological sections were compiled by scanning hand drafts as black and white TIF files, and then digitising the linework using the Corel Draw X3 graphics package. By using the GIS Data processing application Global Mapper 12, contour lines for the 1:10,000 scale topographic base map were generated from digital elevation models (DEMs) based on the Shuttle Radar Topography Mission 26 (SRTM) as released by the United States Geological Survey (SRTM3 USGS version 2.1).

Acknowledgements

The logistics of fieldwork were greatly assisted by Mario Urbina (Museo de Historia Natural, Universidad Nacional

Mayor de San Marcos, Lima). Journal reviewers Mike Shand, Domenico Chiarella, Felipe Torres Figueiredo, Andre Marconato and Associate Editor Claudio Riccomini are gratefully acknowledged for their thoughtful contribution and helpful criticism that sharpened the focus of this study.








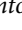

Disclosure statement

No potential conflict of interest was reported by the authors.

Funding

Fieldwork expenses and costs of the Article Publishing Charge for this study were supported by grants from the Italian Ministero dell'Istruzione, dell'Università e della Ricerca (MIUR) to Bianucci (PRIN Project, 2012YJSBMK EAR-9317031), Malinverno (PRIN Project, 2012YJSBMK_002), Di Celma (PRIN Project, 2012YJSBMK_003; FFABR 2017 grant), National Geographic Society Committee for Research Exploration to Bianucci (9410-13), and the University of Pisa to Bianucci (PRA_2017_0032).

ORCID

Claudio Di Celma  <http://orcid.org/0000-0001-7781-7981>
 Elisa Malinverno  <http://orcid.org/0000-0002-9124-5155>
 Giulia Bosio  <http://orcid.org/0000-0001-8067-4926>
 Karen Gariboldi  <http://orcid.org/0000-0002-7978-7496>
 Alberto Collareta  <http://orcid.org/0000-0002-6513-8882>
 Anna Gioncada  <http://orcid.org/0000-0002-8513-7377>
 Walter Landini  <http://orcid.org/0000-0001-7196-9888>
 Pietro Paolo Pierantoni  <http://orcid.org/0000-0002-1237-4689>
 Giovanni Bianucci  <http://orcid.org/0000-0001-7105-0863>

References

- Barron, J. A. (2003). Planktonic marine diatom record of the past 18 my: Appearances and extinctions in the Pacific and Southern Oceans. *Diatom Research*, 18, 203–224. doi:10.1080/0269249X.2003.9705588
- Bianucci, G., Di Celma, C., Collareta, A., Landini, W., Post, K., Tinelli, C., ... Lambert, O. (2016). Fossil marine vertebrates of Cerro Los Quesos: Distribution of cetaceans, seals, crocodiles, seabirds, sharks, and bony fish in a late Miocene locality of the Pisco Basin, Peru. *Journal of Maps*, 12, 1037–1046. doi:10.1080/17445647.2015.1115785
- Bianucci, G., Di Celma, C., Landini, W., Post, K., Tinelli, C., de Muizon, C., ... Lambert, O. (2016). Distribution of fossil marine vertebrates in Cerro Colorado, the type locality of the giant raptorial sperm whale *Livyatan melvillei* (Miocene, Pisco Formation, Peru). *Journal of Maps*, 12, 543–557. doi:10.1080/17445647.2015.1048315
- Bianucci, G., Di Celma, C., Urbina, M., & Lambert, O. (2016). New beaked whales from the late Miocene of Peru and evidence for convergent evolution in stem and crown Ziphiidae (Cetacea, Odontoceti). *PeerJ*, 4, e2479. doi:10.7717/peerj.2479
- Bishop, B. T., Beck, S. L., Zandt, G., Wagner, L., Long, M., Antonijevic, S. K., ... Tavera, H. (2017). Causes and consequences of flat-slab subduction in southern Peru. *Geosphere*, 13, 1392–1407. doi:10.1130/GES01440.1

- Boessenecker, R. W., Perry, F. A., Schmitt, J. G., & Farke, A. A. (2014). Comparative taphonomy, taphofacies, and bonebeds of the Mio-Pliocene Purisima Formation, Central California: Strong physical control on marine vertebrate preservation in shallow marine settings. *PLoS ONE*, 9, e91419. doi:10.1371/journal.pone.0091419
- Bosio, G., Gioncada, A., Malinverno, E., Di Celma, C., Villa, I.M., Cataldi, G., Gariboldi, K., Collareta, A., Urbina, M., & Bianucci, G. (in press). Chemical and petrographic fingerprinting of volcanic ashes as a tool for high-resolution stratigraphy of the upper Miocene Pisco Formation (Peru). *Journal of the Geological Society*. doi:10.1144/jgs2018-071
- Brand, L. R., Esperante, R., Chadwick, A. V., Porras, O. P., & Alomía, M. (2004). Fossil whale preservation implies high diatom accumulation rate in the Miocene–Pliocene Pisco Formation of Peru. *Geology*, 32, 165–168. doi:10.1130/G20079.1
- Brand, L., Urbina, M., Chadwick, A., DeVries, J. T., & Esperante, R. (2011). A high resolution stratigraphic framework for the remarkable fossil cetacean assemblage of the Miocene/Pliocene Pisco Formation, Peru. *Journal of South American Earth Sciences*, 31, 414–425. doi:10.1016/j.jsames.2011.02.015
- Chiarella, D., Longhitano, S. G., & Tropeano, M. (2017). Types of mixing and heterogeneities in siliciclastic-carbonate sediments. *Marine and Petroleum Geology*, 88, 617–627. doi:10.1016/j.marpetgeo.2017.09.010
- Chiocci, F. L., & Clifton, H. E. (1991). Gravel-filled gutter casts in nearshore facies – Indicators of ancient shoreline trend. In R. H. Osborne (Ed.), *From Shoreline to Abyss: Contributions in marine geology in honor of Francis Parker Shepard* (pp. 67–76). Tulsa, OK: SEPM Spec. Publ. 46.
- Clift, P. D., Pecher, I., Kukowski, N., & Hampel, A. (2003). Tectonic erosion of the Peruvian forearc, Lima Basin, by subduction and Nazca Ridge collision. *Tectonics*, 22, 1023. doi:10.1029/2002TC001386
- Coira, B., Davidson, J., Mpodozis, C., & Ramos, V. (1982). Tectonic and magmatic evolution of the Andes of northern Argentina and Chile. *Earth-Science Reviews*, 18, 303–332. doi:10.1016/0012-8252(82)90042-3
- Collareta, A., Landini, W., Chacaltana, C., Valdivia, W., Altamirano-Sierra, A., Urbina-Schmitt, M., & Bianucci, G. (2017). A well preserved skeleton of the fossil shark *Cosmopolitodus hastalis* from the late Miocene of Peru, featuring fish remains as fossilized stomach contents. *Rivista Italiana di Paleontologia e Stratigrafia*, 123, 11–22. doi:10.13130/2039-4942/8005
- Collareta, A., Landini, W., Lambert, O., Post, K., Tinelli, C., Di Celma, C., ... Bianucci, G. (2015). Piscivory in a Miocene Cetotheriidae: first record of fossilized stomach content for an extinct baleen-bearing whale. *The Science of Nature*, 102. doi:10.1007/s00114-015-1319-y
- DeVries, T. J. (1998). Oligocene deposition and Cenozoic sequence boundaries in the Pisco Basin (Peru). *Journal of South American Earth Sciences*, 11, 217–231. doi:10.1016/S0895-9811(98)00014-5
- DeVries, T. J., & Jud, N. A. (2018). Lithofacies patterns and paleogeography of the Miocene Chilcatay and lower Pisco depositional sequences (East Pisco Basin, Peru). *Bol. Soc. Geol. Perú*, 8, 124–167.
- DeVries, T. J., Urbina, M., & Jud, N. A. (2017). The Eocene–Oligocene Otuma depositional sequence (East Pisco Basin, Peru): Paleogeographic and paleoceanographic implications of new data. *Bol. Soc. Geol. Perú*, 112, 14–38.
- Di Celma, C., Malinverno, E., Bosio, G., Collareta, A., Gariboldi, K., Gioncada, A., ... Bianucci, G. (2017). Sequence stratigraphy and paleontology of the Upper Miocene Pisco Formation along the western side of the lower Ica Valley (Ica Desert, Peru). *Rivista Italiana di Paleontologia e Stratigrafia (Research in Paleontology and Stratigraphy)*, 123, 255–273.
- Di Celma, C., Malinverno, E., Cantalamessa, G., Gioncada, A., Bosio, G., Villa, I. M., ... Bianucci, G. (2016). Stratigraphic framework of the late Miocene Pisco Formation at Cerro Los Quesos (Ica Desert, Peru). *Journal of Maps*, 12, 1020–1028. doi:10.1080/17445647.2015.1115783
- Di Celma, C., Malinverno, E., Collareta, A., Bosio, G., Gariboldi, K., Lambert, O., ... Bianucci, G. (2018). Facies analysis, stratigraphy and marine vertebrate assemblage of the lower Miocene Chilcatay Formation at Ullujaya (Pisco basin, Peru). *Journal of Maps*, 14, 257–268. doi:10.1080/17445647.2018.1456490
- Di Celma, C., Malinverno, E., Gariboldi, K., Gioncada, A., Rustichelli, A., Pierantoni, P. P., ... Bianucci, G. (2016). Stratigraphic framework of the late Miocene to Pliocene Pisco Formation at Cerro Colorado (Ica Desert, Peru). *Journal of Maps*, 12, 515–529. doi:10.1080/17445647.2015.1047906
- Di Celma, C., Ragaini, L., Cantalamessa, G., & Curzio, P. (2002). Shell concentrations as tools in characterizing sedimentary dynamics at sequence-bounding unconformities: Examples from the lower unit of the Canoa Formation (Late Pliocene, Ecuador). *Geobios*, 35, 72–85. doi:10.1016/S0016-6995(02)00049-9
- Dunbar, R. B., Marty, R. C., & Baker, P. A. (1990). Cenozoic marine sedimentation in the Sechura and Pisco basins, Peru. *Palaeogeography, Palaeoclimatology, Palaeoecology*, 77, 235–261. doi:10.1016/0031-0182(90)90179-B
- Eberli, G. P., Anselmetti, F. S., Kroon, D., Sato, T., & Wright, J. D. (2002). The chronostratigraphic significance of seismic reflections along the Bahamas Transect. *Marine Geology*, 185, 1–17. doi:10.1016/S0025-3227(01)00287-0
- Esperante, R., Brand, L. R., Chadwick, A. V., & Poma, O. (2015). Taphonomy and paleoenvironmental conditions of deposition of fossil whales in the diatomaceous sediments of the Miocene/Pliocene Pisco Formation, southern Peru—A new fossil-lagerstätte. *Palaeogeography, Palaeoclimatology, Palaeoecology*, 417, 337–370. doi:10.1016/j.palaeo.2014.09.029
- Esperante, R., Brand, L. R., Nick, K. E., Poma, O., & Urbina, M. (2008). Exceptional occurrence of fossil baleen in shallow marine sediments of the Neogene Pisco Formation, Southern Peru. *Palaeogeography, Palaeoclimatology, Palaeoecology*, 257, 344–360. doi:10.1016/j.palaeo.2007.11.001
- Flower, B. P., & Kennett, J. P. (1994). The middle Miocene climate transition: East Antarctic ice sheet development, deep ocean circulation and global carbon cycling. *Palaeogeography, Palaeoclimatology, Palaeoecology*, 108, 537–555. doi:10.1016/0031-0182(94)90251-8
- Föllmi, K. B. (2016). Sedimentary condensation. *Earth-Science Reviews*, 152, 143–180.
- Gariboldi, K. (2016). A note on diatom stratigraphic markers in upper Miocene sediments of the Pisco Formation, Peru, and description of *Delphineis urbinai* sp. nov. *Diatom Research*, 31, 285–301. doi:10.1080/0269249X.2016.1220984
- Gariboldi, K., Bosio, G., Malinverno, E., Gioncada, A., Di Celma, C., Villa, I. M., ... Bianucci, G. (2017). Biostratigraphy, geochronology and sedimentation rates of the upper Miocene Pisco Formation at two important marine vertebrate fossil-bearing sites of southern Peru.

- Newsletters on Stratigraphy*, 50, 417–444. doi:10.1127/nos/2017/0345
- Gariboldi, K., Gioncada, A., Bosio, G., Malinverno, E., Di Celma, C., Tinelli, C., ... Bianucci, G. (2015). The dolomite nodules enclosing fossil marine vertebrates in the East Pisco Basin, Peru: Field and petrographic insights into the Lagerstätte formation. *Palaeogeography, Palaeoclimatology, Palaeoecology*, 438, 81–95. doi:10.1016/j.palaeo.2015.07.047
- Gioncada, A., Collareta, A., Gariboldi, K., Lambert, O., Di Celma, C., Bonaccorsi, E., ... Bianucci, G. (2016). Inside baleen: Exceptional microstructure preservation in a late Miocene whale skeleton from Peru. *Geology*, 44, 839–842. doi:10.1130/G38216.1
- Gioncada, A., Gariboldi, K., Collareta, A., Di Celma, C., Bosio, G., Malinverno, E., ... Bianucci, G. (2018). Looking for the key to preservation of fossil marine vertebrates in the Pisco Formation of Peru: New insight from a small dolphin skeleton. *Andean Geology*, 45, 379–398. doi:10.5027/andgeoV45n3-3122
- Gioncada, A., Petrini, R., Bosio, G., Gariboldi, K., Collareta, A., Malinverno, E., ... Bianucci, G. (2018). Insights into the diagenetic environment of fossil marine vertebrates of the Pisco Formation (late Miocene, Peru) from mineralogical and Sr-isotope data. *Journal of South American Earth Sciences*, 81, 141–152. doi:10.1016/j.jsames.2017.11.014
- Grimm, K. A. (2000). Stratigraphic condensation and the redeposition of economic phosphorite: Allostratigraphy of Oligo-Miocene shelfal sediments, Baja California Sur, Mexico. In C. R. Glenn, L. Prévôt-Lucas, & J. Lucas (Eds.), *Marine Authigenesis: From microbial to global* (pp. 325–347). Tulsa, OK: SEPM Spec. Publ., 66.
- Hampel, A., Kukowski, N., Bialas, J., Huebscher, C., & Heinbockel, R. (2004). Ridge subduction at an erosive margin: The collision zone of the Nazca Ridge in southern Peru. *Journal of Geophysical Research: Solid Earth*, 109, 297. doi:10.1029/2003JB002593
- Holbourn, A., Kuhnt, W., Clemens, S., Prell, W., & Andersen, N. (2013). Middle to late Miocene stepwise climate cooling: Evidence from a high-resolution deep water isotope curve spanning 8 million years. *Paleoceanography*, 28, 688–699. doi:10.1002/2013PA002538
- Hsu, J. T. (1992). Quaternary uplift of the Peruvian coast related to the subduction of the Nazca Ridge: 13.5 to 15.6° south latitude. *Quaternary International*, 15/16, 87–97. doi:10.1016/1040-6182(92)90038-4
- John, C. M., Karner, G. D., Browning, E., Leckie, R. M., Mateo, Z., Carson, B., & Lowery, C. (2011). Timing and magnitude of Miocene eustasy derived from the mixed siliciclastic-carbonate stratigraphic record of the north-eastern Australian margin. *Earth and Planetary Science Letters*, 304, 455–467. doi:10.1016/j.epsl.2011.02.013
- John, C. M., Karner, G. D., & Mutti, M. (2004). $\delta^{18}\text{O}$ and Marion Plateau backstripping: Combining two approaches to constrain late middle Miocene eustatic amplitude. *Geology*, 32, 829–832. doi:10.1130/G20580.1
- Kulm, L. D., Resig, J. M., Thornburg, T. M., & Schrader, H.-J. (1982). Cenozoic structure, stratigraphy and tectonics of the central Peru forearc. In J. K. Leggett (Ed.), *Trench-Forearc Geology: Sedimentation and tectonics on modern and ancient active plate margins* (pp. 151–169). London: Geological Society, Special Publications, 10. doi:10.1144/GSL.SP.1982.010.01.10
- Lambert, O., Bianucci, G., Post, K., de Muizon, C., Salas-Gismondi, R., Urbina, M., & Reumer, J. (2010). The giant bite of a new raptorial sperm whale from the Miocene epoch of Peru. *Nature*, 466, 105–108. doi:10.1038/nature09067
- Lambert, O., Bianucci, G., Urbina, M., & Geisler, J. H. (2017). A new inioid (Cetacea, Odontoceti, Delphinidae) from the Miocene of Peru and the origin of modern dolphin and porpoise families. *Zoological Journal of the Linnean Society*, 179, 919–946. doi:10.1111/zoj.12479
- Lambert, O., Collareta, A., Landini, W., Post, K., Ramassamy, B., Di Celma, C., ... Bianucci, G. (2015). No deep diving: Evidence of predation on epipelagic fish for a stem beaked whale from the late Miocene of Peru. *Proceedings of the Royal Society of London Part B: Biological Sciences*, 282, article no. 20151530. doi:10.1098/rspb.2015.1530
- Landini, W., Altamirano-Sierra, A., Collareta, A., Di Celma, A., Urbina, M., & Bianucci, G. (2017). The late Miocene elasmobranch assemblage from Cerro Colorado (Pisco Formation, Peru). *Journal of South American Earth Sciences*, 73, 168–190. doi:10.1016/j.jsames.2016.12.010
- Landini, W., Collareta, A., Pesci, F., Di Celma, C., Urbina, M., & Bianucci, G. (2017). A secondary nursery area for the copper shark *Carcharhinus brachyurus* from the late Miocene of Peru. *Journal of South American Earth Sciences*, 78, 164–174. doi:10.1016/j.jsames.2017.07.003
- Leckie, D. A., & Walker, R. G. (1982). Storm- and tide-dominated shorelines in Cretaceous Moosebar-Lower Gates interval: Outcrop equivalents of deep basin gas trap in western Canada. *American Association of Petroleum Geologists Bulletin*, 66, 138–157.
- León, W., Aleman, A., Torres, V., Rosell, W., & De La Cruz, O. (2008). Estratigrafía, sedimentología y evolución tectónica de la cuenca Pisco Oriental. *Boletín INGEMMET*, 27 (Serie D), 144. Lima, Peru.
- MacEachern, J. A., Raychaudhuri, I., & Pemberton, S. G. (1992). Stratigraphic applications of the *Glossifungites* ichnofacies: Delineating discontinuities in the rock record. In S. G. Pemberton (Ed.), *Applications of ichnology to petroleum exploration* (pp. 169–198). Tulsa, OK: SEPM Core Workshop Notes 17.
- Macharé, J., & Ortlieb, L. (1992). Plio-Quaternary vertical motions and the subduction of the Nazca Ridge, central coast of Peru. *Tectonophysics*, 205, 97–108. doi:10.1016/0040-1951(92)90420-B
- Marx, F. G., Collareta, A., Gioncada, A., Post, K., Lambert, O., Bonaccorsi, E., ... Bianucci, G. (2017). How whales used to filter: Exceptionally preserved baleen in a Miocene cetotheriid. *Journal of Anatomy*, 231, 212–220. doi:10.1111/joa.12622
- Marx, F. G., Lambert, O., & de Muizon, C. (2017). A new Miocene baleen whale from Peru deciphers the dawn of cetotheriids. *Royal Society Open Science*, 4, 170560. doi:10.1098/rsos.170560
- Massari, F., & D'Alessandro, A. (2012). Facies partitioning and sequence stratigraphy of a mixed siliciclastic-carbonate ramp stack in the Gelasian of Sicily (S Italy): A potential model for icehouse, distally-steepened heterozoan ramps. *Rivista Italiana di Paleontologia e Stratigrafia*, 118, 503–534. doi:10.13130/2039-4942/6017
- Miller, K. G., Mountain, G. S., Browning, J. V., Kominz, M., Sugarman, P. J., Christie-Blick, N., ... Wright, J. D. (1998). Cenozoic global sea level, sequences, and the New Jersey transect; results from coastal plain and continental slope drilling. *Reviews of Geophysics*, 36, 569–601. doi:10.1029/98RG01624
- Miller, K. G., Wright, J. D., & Fairbanks, R. G. (1991). Unlocking the Ice House: Oligocene-Miocene oxygen isotopes, eustasy, and margin erosion. *Journal of Geophysical*

- Research: Solid Earth*, 96(B4), 6829–6848. doi:10.1029/90JB02015
- Mukasa, S. B., & Henry, D. J. (1990). The San Nicolás batholith of coastal Peru: Early Palaeozoic continental arc or continental rift magmatism? *Journal of the Geological Society*, 147, 27–39. doi:10.1144/gsjgs.147.1.0027
- Myrow, P. M. (1992). Pot and gutter casts from the Chapel Island Formation, southeast Newfoundland. *Journal of Sedimentary Research*, 62, 992–1007. doi:10.2110/jsr.62.992
- NACSN. (2005). North American stratigraphic code. *AAPG Bulletin*, 89, 1547–1591. doi:10.1306/07050504129
- Pomar, L., & Tropeano, M. (2001). The Calcarene di Gravina Formation in Matera (southern Italy): New insights for coarse-grained, large scale, cross-bedded bodies encased in offshore deposits. *American Association of Petroleum Geologists Bulletin*, 85, 661–689. doi:10.1306/8626C979-173B-11D7-8645000102C1865D
- Rustichelli, A., Di Celma, C., Tondi, E., Baud, P., & Vinciguerra, S. (2016). Fibrous gypsum veins as diffuse features and within fault zones: The case study of the Pisco Basin (Ica desert, southern Peru). *Journal of the Geological Society*, 173, 405–418. doi:10.1144/jgs2015-084
- Rustichelli, A., Di Celma, C., Tondi, E., & Bianucci, G. (2016). Deformation within the Pisco basin sedimentary record (southern Peru): Stratabound orthogonal vein sets and their impact on fault development. *Journal of South American Earth Sciences*, 65, 79–100. doi:10.1016/j.jsames.2015.11.002
- Thornburg, T. M., & Kulm, L. D. (1981). Sedimentary basins of the Peru continental margin: Structure, stratigraphy, and Cenozoic tectonics from 6°S to 16°S latitude. In L. D. Kulm, J. Dymond, E. J. Dasch, & D. M. Hussong (Eds.), *Nazca plate: Crustal formation and Andean convergence* (pp. 393–422). Tulsa, OK: Geological Society of America, *Memoir*, 154.
- Turco, E., Hilgen, F. J., Lourens, L. J., Shackleton, N. J., & Zachariasse, W. J. (2001). Punctuated evolution of global climate cooling during the late Middle to early Late Miocene: High-resolution planktonic foraminiferal and oxygen isotope records from the Mediterranean. *Paleoceanography*, 16, 405–423. doi:10.1029/2000PA00050
- Viveen, W., & Schlunegger, F. (2018). Prolonged extension and subsidence of the Peruvian forearc during the Cenozoic. *Tectonophysics*, 730, 48–62. doi:10.1016/j.tecto.2018.02.018
- Westerhold, T., Bickert, T., & Röhl, U. (2005). Middle to late Miocene oxygen isotope stratigraphy of ODP site 1085 (SE Atlantic): New constrains on Miocene climate variability and sea-level fluctuations. *Palaeogeography, Palaeoclimatology, Palaeoecology*, 217, 205–222. doi:10.1016/j.palaeo.2004.12.001
- Zachos, J. C., Shackleton, N. J., Revenaugh, J. S., Pälike, H., & Flower, B. P. (2001). Climate response to orbital forcing across the Oligocene-Miocene boundary. *Science*, 292, 274–278. doi:10.1126/science.1058288